REALIZATION OF FTA WITH HIGH TRACKING ACCURACY IN FSO

Chun Lei Lv, Yan Li, Yun Feng Zhang, Hui Lin Jiang, and Shou Feng Tong

ABSTRACT

High tracking accuracy is a prerequisite of reliable space optical communication links and its effective means is the utilization of coarse and fine compound-axis structure. After an in-depth study of the active laser tracking mechanism of fine tracking assembly, this paper emphasizes the exploration of these methods enabling the improvement of tracking accuracy under the condition of relative movement and platform vibration. Firstly, switching technique using a single beacon between different divergence angles is put forward to improve the signal to noise ratio (SNR) of the focal spot. Secondly, the high-frame rate charge-coupled device is achieved after proposing the pseudo random window readout technique. Thirdly, the unique design of the high resonant frequency of two-dimensional PZT fast steering mirror (FSM) and sub-pixel subdivision technique with adaptive control of integral time is used to achieve high accuracy and fast beam pointing. Fourthly, this paper puts forward a digital servol control method with intelligent variable structure. Finally, after building a hardware-in-loop simulation platform, the tracking accuracy of 3µrad is concluded according to simulation experimental results.

Key Words: Compound-axis, servo control system, fine tracking assembly (FTA), tracking accurary, free-space optical communication (FSO).

I. INTRODUCTION

Diffraction-limited laser beams are usually required for long-haul space laser communication with low power consumption and high data-rate. For inter-satellite links (ISL), a typical divergence angle of beam is only about 20µrad [1]. Moreover, the optical power distribution of far-field laser beam is approximate to the Gauss model [2], and the power density at the center of the axis is the largest. Therefore, in order to reduce the power loss of communication beam induced by the Acquisition Pointing and Tracking (APT) tracking error, it is necessary to accurately point the communication beams between both optical terminals. Axis pointing accuracy of less than one-eighth of a communication beam divergence angle (2~3µrad) can ensure that power loss caused by the APT tracking error is less than 0.5 dB [3]. Thus, dynamic and high tracking accuracy under the condition of relative motion and platform vibration is indispensable to establish reliable space laser communication links. In previous papers [4,5], some methods were proposed. However, some questions arose in the course of a 50 km field laser communication experiment in

2012 and a subsequent 150 km laser communication experiment between both aircrafts in October 2013. Servo control units cannot well work in motor-vibrating aircrafts and spot detection accuracy is beyond 0.33µrad, which results in failure of the tracking accuracy of 3µrad in the real field environment.

II. ANALYSIS OF DECISIVE FACTORS OF TRACKING ACCURACY

The tracking accuracy of the compound-axis APT subsystem finally depends on fine tracking assembly (FTA) [6], whose structure is shown in Fig. 1. According to the principle of automatic control system, a high bandwidth of tracking system, not only can reduce dynamic delay error, but also well suppresses well the wide spectrum, colored noise [7]. In particular, the better the effect of vibration suppression, the greater the ratio between the tracking bandwidth and spectral width of platform vibration is greater, the better the effect of vibration suppression is. The higher the servo stiffness is, the better the effect of vibration suppression is. Thus, increasing the bandwidth of the tracking system is an important way to reduce tracking error [8]. However, for this broadband and active photoelectric tracking system, except apart from reliability and robustness, high resonant frequency servo mechanism and high sampling frequency, high accuracy of miss distance detection unit is also absolutely necessary; herein which the design difficulty just lies.
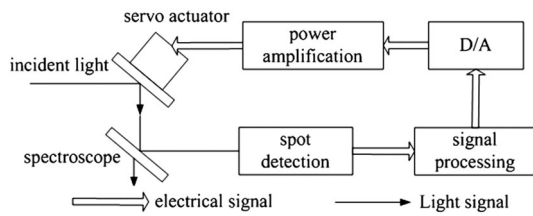
Fig. 1. Fine tracking assembly of compound axis.

To achieve the high sampling frequency of the miss distance detection unit, first a charge-coupled device (CCD) camera needs to work with high-frame frequency, because in the course of spot detection and signal processing, there is a certain delay time, which decreases the phase margin of the control system [9], and thus influences system bandwidth and stability. In order to minimize the impact of the delay time on control systems, the frame rate of area array CCD is required to reach a servo bandwidth of more than 10 times. Generally a closed-loop bandwidth of 10Hz~15Hz can just meet the accuracy requirement of the coarse tracking assembly (CTA) [10]. However, in order to effectively correct the residual error of CTA, FTA bandwidth is required to have a CTA bandwidth of more than 20 times. So, a closed-loop bandwidth of FTA will reach 300Hz and therefore the frame rate of CCD will be up to 3000Hz, which inevitably results in a minimal CCD integral time. Consequently, a beacon of high-power density is required to achieve a high SNR of spots. In view of the above major problems, this article puts forward corresponding methods.

III. SOLUTIONS TO KEY TECHNOLOGIES

3.1. Switching technique using a single beacon between different divergence angles

The compound-axis APT subsystem requires a larger beacon divergence angle and tracking FOV (field of view) to reduce the time of open-loop pointing and capturing. After closed-loop tracking between both optical terminals, in which time fine tracking begins to work and a communication link is subsequently established, a high-frame rate CCD of 3000Hz will be needed in order to increase the bandwidth and tracking accuracy of FTA. Consequently, there is minimal integral time, which results in the demand for a higher-power density of beacon to increase the SNR of the optical spot of CCD. However, the decrease in the beacon divergence angle can greatly enhance the power density.

It is necessary that the divergence angle of the coarse beacon is larger than the uncertainty area of open-loop capturing, ordinarily 10mrad. But there is a relatively long integral time of CCD for coarse tracking and therefore its

power is enough. The divergence angle of the fine beacon is 1mrad and leads to 1:100 ratio of power density between both, which can meet the requirement of minimal integral time of CCD for fine tracking. Therefore, the switching technique between both divergence angles (fine beacon and coarse) using a single beacon is proposed, which reduces the complexity of optical terminals. This switching of divergence angle from 10mard to 1mrad is done by inserting a single group of zoom lenses into a fixed optical path at the time of open-loop capturing. The system then enters closed-loop tracking mode. The transient mode between open-loop capturing and closed-loop tracking can be ignored because the switching is driven by a quick response linear motor in less than 10 milliseconds (as shown in Fig. 2 and Fig. 3) and therefore the captured optical spot cannot move out of sight. When there isn't a group of zoom lenses in the optical path, and all optical components are fixed, 1mrad of fine beacon is transmitted; otherwise 10mrad of coarse one is transmitted. Such a design has taken into account the factors as follows. Firstly, this system is in the working state of closed-loop fine tracking most of the time for the maintenance of a stable communication link and therefore fine beacon is used for a long time, while coarse beacon is only maintained for several seconds at the beginning of capturing. Secondly, the coaxial accuracy between fine tracking LOS (line-of-sight) and communication LOS is higher, but the requirement of coarse beacon is relatively low, so the minimal direction change of LOS caused by inserting the zoom lens can be ignored.

3.2. Implementation of high-frame rate CCD

The mathematical models of the CCD spot detection unit and the video signal-processing unit include a proportional part of limited field of view K_{CCD}, delay part caused by image processing $e^{-\tau s}$ (τ is the time delay induced by the generation of image signal, signal processing, data transmission, and other causes) and sample-and-hold part $\frac{1-e^{\tau_0 s}}{s}$ (τ_0 is the image holding time of every CCD frame) [11]. In order to reduce the impacts of the CCD spot detection unit and the video signal-processing unit on the digital servo unit, the frame rate of CCD is required to reach a closed-loop
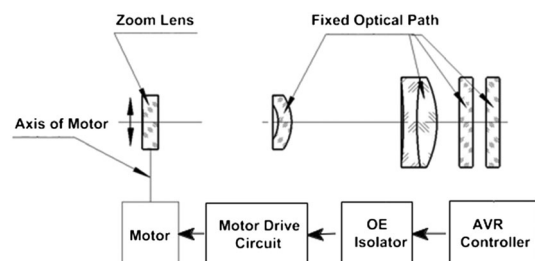

Fig. 2. Coarse/fine beacon switching illustration.

Fig. 3. Coarse/fine beacon switching equipment.

bandwidth of more than 10 times, which results in a phase margin reduction of no more than 5.7° [12] and a smaller impact on the stability of FTA. The pixel readout rate of the CCD has an upper limit due to technical limitations [13]. This means that an ordinary area array CCD is not feasible to achieve a simultaneous high-frame rate and high resolution. FTA requires such a CCD with a low resolution of 80×80 and a high-frame rate of 3000Hz. Inspired by the window of interest random readout technique of CMOS, a pseudo random window readout technique of CCD for achieving a high-frame rate is proposed, which is based on a full understanding of the working characteristics of FTA and the operating principle of CCD. The reason why this technique is named 'pseudo' is derived from the operating principle of CCD, because it is still a serial sequence readout but different from the common timing sequence of area array CCD. The schematic and readout timing sequence is indicated in Fig. 4.

A local area of 80×80 is defined in the lower right corner of the ordinary area array CCD with pixel resolution of 1024×1024, which acts as an effective window of FTA, as shown in area 3 of Fig. 4. This area is driven by a normal timing sequence, while the other pixels of the same line are read out with a rapid timing sequence as shown in area 2.

Similarly, this rapid timing sequence is used for the other out of area lines of FTA in area 1. Through the novel design of the timing sequence and signal processing, a higher speed readout of these invalid areas with a large proportion can greatly improve the frame rate.

In order to realize this theory, a high sensitivity area array CCD with saturation automatic overflow and processing transfer is used [14]. Embedded FPGA is then used to perform special timing sequence control of CCD and an appropriate video signal processing chip is used for image processing. Finally, an intelligent digital CCD camera with variable window number and frame rate of up to 3000Hz is developed, which greatly improves the bandwidth of FTA.

3.3. High resonant frequency servo actuator

Compared to the other drivers, piezoelectric ceramic actuators (PZT), as shown in Fig. 6, with advantages including small volume, high displacement resolution, fast speed of response, large output force, high power conversion efficiency, no heat exchange and displacement of good repeatability in ultra accurate positioning and micro-displacement control, is an ideal driver [15].
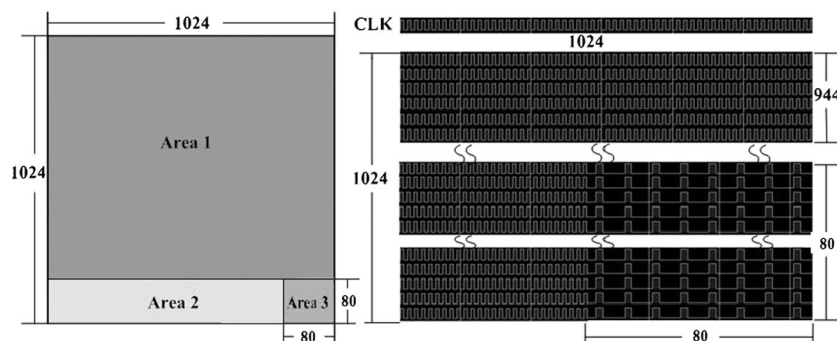

Fig. 4. Operating principle and timing sequence of pseudo random window readout technique.

As shown in Fig. 5, X and Y represent two moving planes of fast steering mirror (FSM); A, B, and C are the three control points of FSM, which also represent its moving distance respectively; b is regarded as the distance between control point A and B; ϕ is the diameter of a circle passing through A, B, C. The formula is as follows

$$a = \frac{b}{2}\sqrt{3}, \phi = \frac{2b}{3}\sqrt{3}$$
$$\theta_x = [A - 1/2(B+C)]/a$$
$$\theta_y = (B-C)/b \qquad (1)$$
$$Z = (A+B+C)/3$$

In this formula, a and b depend on the model of FSM used. θ_x, θ_y, and Z are equivalent to azimuth, pitch angle, and moving distance respectively. According to the above formulas, a voltage change of any point among three control points of FSM will change the inclination degree of the plane, which can be regarded as X and Y, two directions movement. The miss distance of spot can be converted into the analog voltages of A, B, and C control points and then control the movement of FSM[16].

The structure of the FSM servo system consists of a plane reflector, PZT, and its driver. The mathematical model can be obtained using the data fitting method according to the device parameters and experimental test results. Assuming the coupling influence between the X and Y axes is ignored, the movement direction of each axis can be equivalent to a two-order oscillation part. The frequency response analyzer can measure the frequency characteristic curves of azimuth and pitch angle of this controlled object, and after the curve fitting the open-loop transfer function is

$$G_F(s) = \frac{G_{OUT}}{G_{IN}} = \frac{\omega_n^2}{s^2 + 2\zeta\omega_n s + \omega_n^2}$$
$$= \frac{8.9 \times 10^7}{s^2 + 1.3 \times 10^4 s + 8.9 \times 10^7} \qquad (2)$$

Resonant frequency $\omega_n = 2\pi f_n = 9240(rad/\text{sec})$, damping factor $\zeta = 0.7$, G_{OUT} for output, and G_{IN} for input.
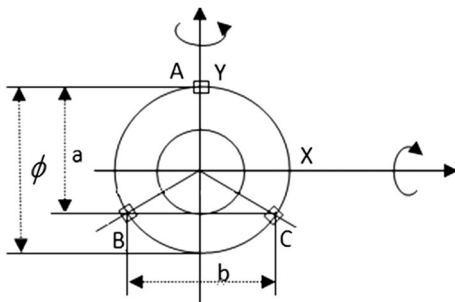
3.4. High accuracy sub-pixel subdivision technique with adaptive control of integral time

Spot detection error is the main source error of FTA. This error, which is slightly enlarged, will be directly transferred to the output end and can't well be suppressed [17], according to control theory. Therefore, improving spot detection accuracy is essential for high-tracking accuracy. Generally, the spot detection error is smaller than 0.33µrad for the microradian tracking system, because the spot detection error needs to be less than the total control error of 1/3. Therefore, under low SNR of focal spot, it is very difficult to implement sub-microradian spot detection.

There are two types of detector available. One is QD (four-quadrant photodiode detector), which has the advantage of high-detection sensitivity and high sampling frequency, but the contradiction inherent in the detection mechanism between the detection range and sensitivity can't be ignored. Therefore, the linearity is poor and it is unfavorable for FTA. The other is the high-frame rate CCD, which is characterized by good linearity and detection sensitivity without the restriction of detection range [18]. Its detection sensitivity only depends on the detection algorithm, power distribution pattern, size, and SNR of focal spot. Consequently, it is used to detect the position of the focal spot.

The sub-pixel subdivision technique is an important method of improving detection accuracy, whose subdivision ability mainly depends on the power distribution pattern, SNR, and the size of the focal spot, background light, and pixel channel width. According to section 3.2, the effective pixels of FTA cannot be more than 80×80. This means that the pixel resolution is only 3µrad, which is very far from the detection accuracy of 0.33µrad. Therefore, a sub-pixel subdivision ability of at least 1/10 is required.

The difficulty of sub-pixel subdivision lies in the following stringent conditions. The low SNR, which is induced by great beacon power loss of long-distance transmission and a minimal integral time of CCD, greatly increases the difficulty of sub-pixel subdivision. In addition, the high angular resolution of FTA caused by long focal length accordingly results in a large radius of a diffraction-limited Aere spot, which will affect the sensitivity of spot centroid detection. Owing to the long focal length of FTA,

Fig. 5. Control principle of PZT.

Fig. 6. PZT.

the spot diameter is close to 20 μm and in excess of CCD pixel size by two times, so that the four-quadrant technique with the highest subdivision ability can't be used.

Therefore, a floating threshold centroid algorithm is proposed to improve the ability of the sub-pixel subdivision. The adaptive control technology of integral time is used to decrease the spot power fluctuation due to the changes of link distance and atmospheric channel attenuation, so that the CCD focal plane array is stably covered by 3–5 pixels and, therefore, the SNR of the detected spot is almost close to a constant value. Consequently, the sub-pixel ability of better than 1/10 pixel is achieved using adaptive control of integral time and centroid algorithm, which ensure the detection accuracy of the 0.33 μrad. Then, embedded FPGA is used for image processing with respect to spot centroid detection, including the calculatiom of adaptive threshold, elimination of random noise, high speed and high accuracy centroid algorithm, and automatic light intensity estimation.

As long as the SNR is enough and the power distribution pattern of spots is sound, higher subdivision accuracy can be obtained. A sub-pixel subdivision accuracy of better than 1/20 pixel has been achieved in our experiment, while [19] has reached 1/50 pixel.

IV. DESIGN OF FTA SERVO SYSTEM

FTA begins to further improve the tracking accuracy in the inner frame after coarse tracking in the outer frame, which is the high bandwidth and high tracking accuracy

of the compound-axis APT system. According to Fig. 1, the principle of the servo control system is shown in Fig. 7.

Position and velocity servo loops are determined to the 2nd-order lead–lag type I system, in which steady-state error is zero for the constant position input, a fixed value for the equal velocity input, and infinity for the equal acceleration input. However, steady-state error is zero for the constant position input and the equal velocity input, and a fixed value for the equal acceleration input in the type II system. Generally, as a result of the weak stability of the type II system, the FTA servo system is designed to type I.

In Fig. 7, Disturb2 represents external disturbance of the coarse-axis from wind and rub resistance. Distrub1 represents external disturbance of the fine-axis from rub resistance and the coupling force between the coarse-axis and the fine-axis.

Adopting the coarse and fine move control mode, the lower part of Fig. 7 is for fine-axis control, and the upper is for coarse-axis control. We can conclude that the expression of the double lags in velocity loop is $\frac{(0.0562s+1)^2}{(2.08s+1)^2}$ and the expression of the lag in position loop is $\frac{0.417s+1}{2.632s+1}$. Similarly, we can conclude that the expression of the double lags in velocity loop is $\frac{(0.357s+1)^2}{(3.125s+1)^2}$ and the expression of the lag in position loop is $\frac{0.56s+1}{5.26s+1}$.

In order to improve the steady-state performance of the system, we can use the high-frequency amplitude correction
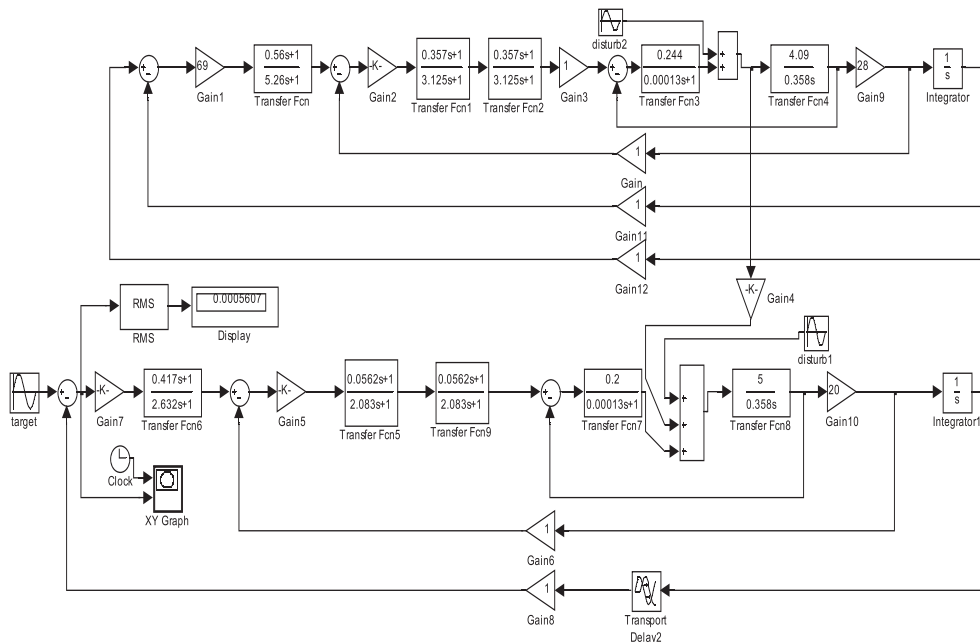

Fig. 7. Control principle block diagram of FTA.

network lag (high frequency Amplitude attenuation) attenuation characteristic to correct the original system's low frequency part. This method is called series-connected lead correction in the frequency domain. As a result of reducing the amplitude of the crossover frequency, the system bandwidth is smaller, thereby reducing the response speed of the system and improving the system's anti-jamming capabilities. There are two reasons why we use this control regulator mode of lead correction. Firstly, lead correction can increase the phase margin to improve the stability of the system. Secondly, lead correction can improve the frequency characteristics of high frequency gain, increase the shear frequency of the system, and broaden the system bandwidth, so that the system can respond more quickly.

The position loop and the speed loop is the same lead–lag mode. The lead correction can increase the phase margin of the system so that the system can improve its dynamic performance. The lag correction can improve its static performance.

The control function of digital compensation is constituted by using the design method of the intelligent variable structure servo system. After spectrum analysis of input signal, the bands of spectrum which need to be suppressed are identified, and then according to control bandwidth and the peak of closed-loop frequency response, each corner frequency of the type I system is calculated. Subsequently, the analog function of the servo control system is given in accordance with corner frequency, and finally it is digitized using the bilinear transformation method. Generally, when the interval between both middle bandwidths of the inner loop and the outer loop is larger, the inner loop can be more easily simplified. In practice, when the bandwidth of the inner loop is more than five times that of the outer loop, the inner loop can be equivalent to an inertial element. When the bandwidth of the inner loop is much larger than that of the outer loop, sometimes it can also be simplified to be a proportional element.

The design of the velocity loop is required to meet the dynamic characteristics of the position loop. Thus, enough open-loop gain, good mechanical characteristics, and governing characteristics are necessary for the velocity loop. These influence the dynamic characteristics of the velocity loop, including the gain, bandwidth, and the form of the transfer function. In order to achieve the required one must determine the parameters of the transfer function. The transfer function of the 2nd-order regulator in the velocity loop is

$$W_2(s) = \frac{11865\left(\frac{1}{8.5}s + 1\right)\left(\frac{1}{93.37}s + 1\right)}{\left(\frac{1}{0.2202}s + 1\right)\left(\frac{1}{79.4}s + 1\right)} \tag{3}$$

The position loop is to achieve stability and dynamic performance under the given velocity and acceleration,

which depend on the sampling frequency and time delay of the sensor, the bandwidth, and open-loop gain of the loop. Lag–lead correction is chosen for the high bandwidth of the position loop, because the fast steering mirror is driven by the high bandwidth of PZT, the resonance frequency of which can be up to several hundred, even thousand, Hz. The transfer function of the 2nd-order regulator in the position loop is

$$W_1(s) = \frac{14400(2s + 1)(2s + 1)}{(20s + 1)(27.28s + 1)} \tag{4}$$

V. HARDWARE-IN-LOOP SIMULATION EXPERIMENT

The servo system performance is characterized by open-loop and closed-loop responses. The open-loop character mainly includes cut-off frequency and phase margin. The former represents steady state error and the latter influences the stability of the system. The closed-loop character represents dynamic performance. The analysis is as follows.

The curve of the open-loop logarithm amplitude-frequency and phase-frequency characteristics is shown in Fig. 8, according to simulation modeling. It is found that the open-loop cut-off frequency of FTA is 333Hz, the phase margin is 65.4°, which is larger than 50° of the practical requirement limit, and the gain that influences the low frequency tracking accuracy is more than 110 dB. This gurantees the stability of the system, and also ensures that the bandwidth and stiffness of the servo unit meets the system's requirements.

The curve of the closed-loop logarithm amplitude-frequency and phase-frequency characteristics is shown in Fig. 9. The closed-loop bandwidth of FTA can approach 600Hz, which meets the system's requirements.
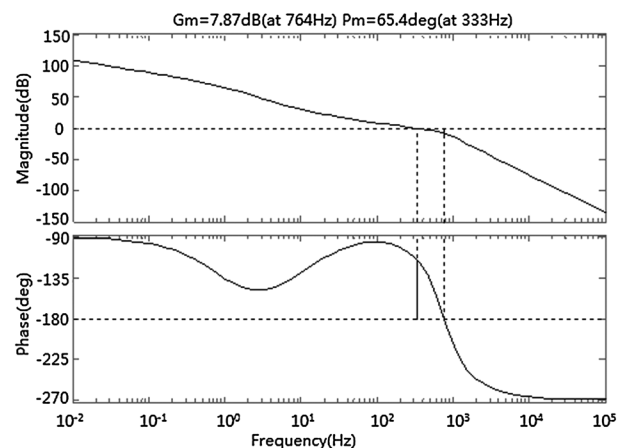

Fig. 8. The curve of open-loop amplitude-frequency and phase-frequency characteristics.

The vibration timing curve, in accordance with the ESA's (European Space Agency) vibration power spectrum density of SILEX (Semi-Conductor Inter Satellite Link Experiment), the first European optical communication terminal in orbit as an input source, is simulated into optical-axis jitter simulation platform with high bandwidth and high accuracy to evaluate the vibration suppression ability of FTA. The simulation platform is characterized by an analog bandwidth of up to 100Hz, a jitter amplitude of greater than $\pm 1°$, and the accuracy of jitter amplitude with better than 2μrad which has the same physical identity of a real vibration experiment. This hardware-in-loop simulation testbed is shown in Fig. 10. Tag 1: integrated FTA servo control unit, which includes image processing for spot detection, servo control, and driver for PZT. Tag 2: high frame rate CCD. Tag 3: CTA CCD. Tag 4: steering mirror. Tag 5: PZT. Tag 6: driver for steering mirror. Tag 7: control computer for CTA servo control.

The time domain curve of the spot miss distance is shown in Fig. 11. After stable tracking of CTA, the residual error is less than FOV of FTA. The spot detection unit of FTA begins to work, but it does not control the servo system. After the residual error of CTA is recorded, the servo system of FTA just begins to work, LOS immediately points to center FOV of FTA, and the miss distance becomes very small. Therefore, a higher tracking accuracy is obtained.

The tracking accuracy of the compound-axis depends on FTA. After FTA further suppresses residual error, the time domain curve of residual error is shown in Fig. 12. It shows that the error statistics of FTA obey Gauss distribution, the variance σ is 0.8μrad, and the maximum tracking error is 2.4μrad (3σ). After suppression of FTA, residual error of CTA is suppressed to less than 3μrad. Data analysis of residual error in the time domain indicates that the residual error of FTA consists of low frequency envelope and
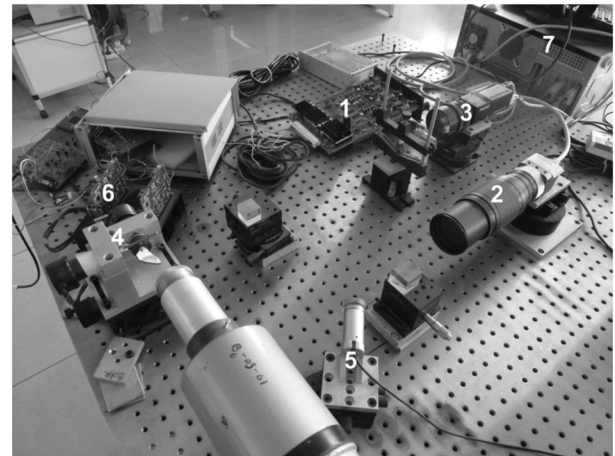

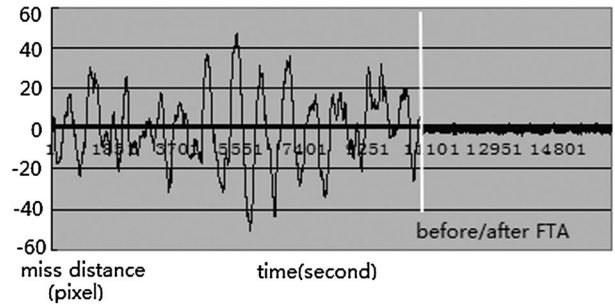Fig. 10. Compound-axis APT testbed for checking tracking error.

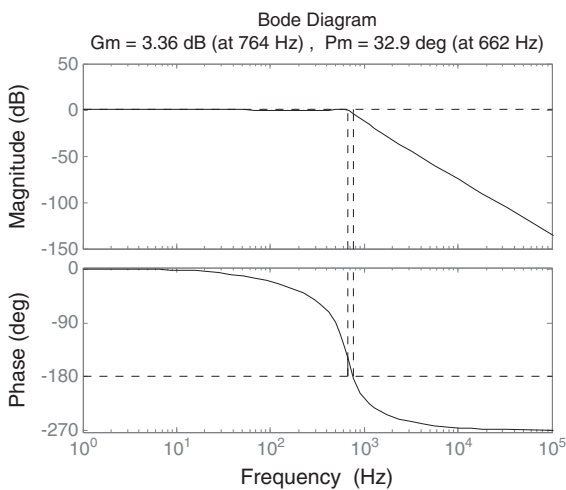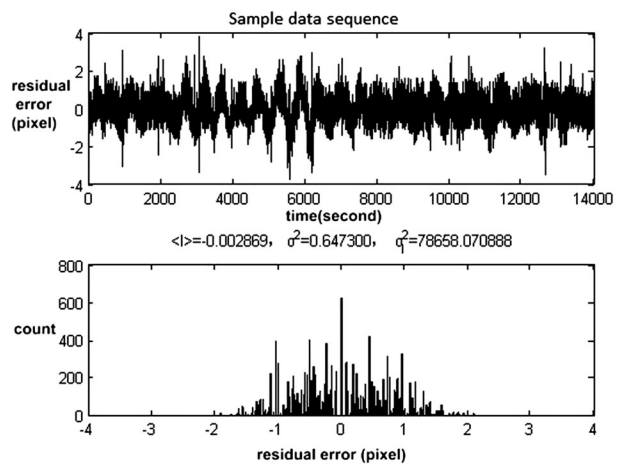Fig. 11. Time domain curve of miss distance before/after FTA works.

Fig. 12. Time domain curve and histogram of FTA residual error.

high frequency noise. The former can be regarded as a dynamic delay error and the latter can be considered as a residual error of platform vibration suppression and spot detection error of CCD.

Fig. 9. The curve of closed-loop amplitude-frequency and phase-frequency characteristics.
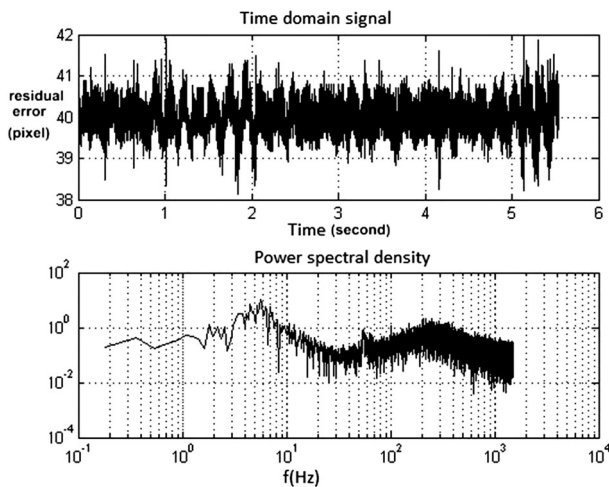
Fig. 13. Time domain curve and its vibration power spectrum of FTA residual error.

Fig. 14. Field laser communication trial between both aircrafts.

The power spectrum of residual error is shown in Fig. 13. This figure shows that there are two peak frequency bandwidths. One is the residual error of CTA of 2 ~6Hz, which relates to the low-frequency envelope of FTA residual error. The other distributes in the band of 200~400Hz and it is caused by bandwidth matching of FTA. They are in accordance with the theoretical analysis and do not cause problems in practice.

VI. CONCLUSION

This paper proposes solutions to four key technologies in the development process of FTA, and demonstrates the building of a hardware-in-loop simulation platform. A tracking accuracy of 3μrad is concluded after an overall performance lab test of FTA and 150 km filed space laser communication trial, which was carried out in October 2013, as shown in Fig. 14. Though these previous methods can meet the requirements of a lab test, some accidents occurred in field trials. After improvements, we are confident in putting forward our ideas.

Therefore, the LOS pointing accuracy requirement of space laser communication is met and can be used as a reference for relevant system design.

REFERENCES

1. Jiang, H. L., S. F. Tong *et al*. *Space Laser Communication Technology*, National Defense Industry Press, Beijing (2010).

2. Hu, S. S. *Automatic Control Theory*, 5th edn., Science Press, Beijing (2011).

3. Nielsen, T. T., and G. Oppenhaeuser, "In orbit test result of an operational inter-satellite link between ARTEMIS and SPOT4, SILEX," *SPIE*, Vol. 4635, pp. 1–15 (2002).

4. Lv, C., H. Jiang, and S. Tong, "Optical-path design and study of fine tracking assembly in space optical communication," 2nd International Conference on Consumer Electronics, Communications and Networks, CECNet 2012, *Proc. IEEE Comput. Soc.*, pp. 1162–116, (2012).

5. Lv, C., H. Jiang, and S. Tong, "Implementation of FTA with high bandwidth and tracking accuracy in FSO," 2nd International Conference on Consumer Electronics, Communications and Networks, CECNet 2012, *Proc. IEEE Comput. Soc.*, pp. 3275–3279 (2012).

6. Gagliardi, R. M. and S. Karp, *Optical Communications*, 2nd edn., John Wiley & Sons, Inc., New York (1995).

7. Zhang, W., and B. Zhu, "The analysis and study of oversampling of CCD in the APT technology of optical communications," *J. Appl. Opt.*, Vol. 25, No. 6, pp. 43–44 (in Chinese) (2005).

8. Masahiro, T., "Acquisition and tracking control of satelliteborne laser communication systems and simulation of downlink fluctuations," *Opt. Eng.*, Vol. 45, No. 8, pp. 4–12 (2006).

9. Li, M., H. Li, and H. Jiang, "Study on fine tracking robust control technology of space laser communication system," *Acta Optica Sinica*, Vol. 29, Supplement, pp. 87–91 (in Chinese) (2009).

10. Lu, N., X. Ke, and H. Zhang, "Research on APT coarse tracking in free-space laser communication," *Infrared and Laser Eng.*, Vol. 39, No. 5, pp. 943–949 (in Chinese) (2010).

11. Tong, S., Y. Liu, and H. Jiang, "Power analysis of APT coarse tracking link of free space laser communication system," *Infrared and Laser Eng.*, Vol. 35, No. 3, pp. 322–325 (in Chinese) (2006).

12. Han, C., B. Bai, X. Zhao *et al*. "Acquisition control system of free space laser communication," *Infrared and*

*Laser Eng.*, Vol. 38, No. 1, pp. 91–95 (in Chinese) (2009).

13. Cao, Y., Y. Ai, M. Li *et al.* "Groundsimulation experiment of fine tracking for spatial optical communication," *J. Optoelectron. Laser*, Vol. 20, No. 1, pp. 40–43 (in Chinese) (2009).

14. Wang, J.-m., Y. Qin, Q. Xu *et al.* "Study on the measurement of tracking and pointing accuracy used for the terminals of free space laser communication," *J. Optoelectron. Laser*, Vol. 19, No. 8, pp. 1054–1059 (in Chinese) (2008).

15. Wang, J.-m., L.-l. Wang, Q. Xu *et al.* "Analysis of the far field distribution measurement of the terminals of free space laser communication and design of the measuring system design," *J. Optoelectron. Laser*, Vol. 19, No. 3, pp. 1467–1473 (in Chinese) (2008).

16. Ding, Tao, G.-l. Xu, X.-p. Zhang *et al.* "Control of bit error rate introduced by platform vibration for free space optical communication," *Chin. Lasers*, Vol. 34, No. 4, pp. 449–502 (2007).

17. Yu, S.-y., Q.-q. Han, J. Ma *et al.* "Size selection of dispersive spot imaging on CCD in a satellite optical communication terminal," *Chin. Lasers*, Vol. 34, No. 1, pp. 67–71 (2007).

18. Liu, N., and J.-H. Chen, "Dual spots detection algorithm of four-quadrant laser guidance," *Infrared and Laser Eng.*, Vol. 39, No. 4, pp. 627–633 (2010).

19. Zhao, X., S.-F. Tong, Y.-Q. Liu *et al.* "Application research on four-quadrant detector in laser communication system," *J. Optoelectron. Laser*, Vol. 21, No. 1, pp. 46–49 (2010).

Chun Lei Lv received his Ph.D. from Changchun Institute of Optics, Fine Mechanics and Physics (CIOMP), Chinese Academy of Sciences in 2009. He is currently Research Assistant at CIOMP. His research interests include servo control, space laser communication, computer image processing and machine vision.
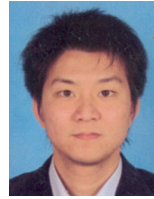
Yan Li received his Ph.D. from Changchun Institute of Optics, Fine Mechanics and Physics (CIOMP), Chinese Academy of Sciences in 2009. He is currently Associate Research Fellow at CIOMP. His research interests include servo control and mechanical design.
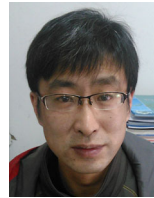
Yun Feng Zhang received the Ph.D. degree from Changchun Institute of Optics, Fine Mechanics and Physics (CIOMP), Chinese Academy of Sciences in 2007. He is currently Research Fellow at CIOMP. His research interest covers computer image processing and machine vision.

Hui Lin Jiang received his Ph.D. from Changchun Institute of Optics, Fine Mechanics and Physics (CIOMP), Chinese Academy of Sciences in 1987. He is currently Professor at Changchun University of Science and Technology. His research interests include space laser communication and optical design.

Shou Feng Tong received his Ph.D. from Changchun Institute of Optics, Fine Mechanics and Physics (CIOMP), Chinese Academy of Sciences in 2000. He is currently Professor at Changchun University of Science and Technology. His research interests include space laser communication, servo control, and optical design.